Available online at www.sciencedirect.com
ScienceDirect
Catalysis Today 120 (2007) 21–29
CATALYSIS TODAY
www.elsevier.com/locate/cattod

From seconds to milliseconds to microseconds through tailored microchannel reactor design of a steam methane reformer

Anna Lee Y. Tonkovich [a,*], Bin Yang [a], Steven T. Perry [a], Sean P. Fitzgerald [a], Yong Wang [b]

[a] *Velocys, Inc., Plain City, OH, United States*
[b] *Pacific Northwest National Laboratory, Richland, WA, United States*

Available online 22 August 2006

Abstract

Conventional steam methane reformers operate with contact times exceeding 1 s. Recent literature has suggested that microchannel reactors may reduce the contact time to a few or tens of milliseconds. This report shows both experimentally and theoretically that the 1 ms barrier for steam methane reforming (SMR) has been broken with the aid of a tailored microchannel reactor design, where the catalyst is coated on a relatively thick porous engineered structure. While 1 ms contact time reactions have been approached by the partial oxidation of methane to synthesis gas, steam reforming has historically been considered a slow reaction. Methane steam reforming experiments at contact times of 90–900 μs were conducted. Greater than 98% approach to equilibrium methane conversion was demonstrated at 900 μs, and 19.7% approach to equilibrium was measured at 90 μs. Both cases were supported with good model agreement. Further, the model explores microchannel reactor structures that minimize heat and mass transfer and results suggest that at a contact time of 500 μs a high approach to equilibrium is possible.

Keywords: Microchannel reactor design; Steam methane reformer; Hydrogen; Millisecond reaction, Microsecond reaction

1. Introduction

Methane steam reforming is the commercial route for producing hydrogen for refining and other high-volume applications. Great interest has been shown over the past decade to find process improvements that reduce both the capital and operating cost of hydrogen production. Microchannel reactors have offered great promise to reduce capital costs by intensifying reactor equipment and to reduce operating costs by improving the system thermal recovery. Recent advancements in process intensification are the topic of this work. A conventional methane steam reformer is quite large, of the order of a 30 m × 30 m × 30 m plant for the production capacity of 20 million standard cubic feet per day (MM SCFD) of hydrogen. The conventional reformer operates with a contact time of the order of 1 s. A microchannel plant with equal capacity has been described in the literature based on a contact time below 10 ms that has a plant volume of 3.9 m × 5.8 m × 3.9 m [1].

This paper will describe experimental and modeling efforts to further intensify the reforming process. The metric of contact time rather than residence time will be explicitly used to more easily compare microchannel reactor performance across many references in a manner that is conducive to future economic comparisons. Further, the contact time basis for the microchannel will be based upon the open channel volume as the reactant flows *by* not *through* the catalyst in a microchannel reactor. One advantage of defining contact time based on the open channel volume is that the effect of catalyst thickness in carefully designed engineered structures can be more easily explored.

Contact times of 900 μs have been experimentally conducted that produce near equilibrium performance and additional modeling has shown how even further reductions in contact time, and thus increases in the overall plant productivity, can be achieved.

2. Background

While 1 ms contact times have been approached for the partial oxidation of methane to syngas, steam reforming has historically been considered a slow reaction [2]. Other reactions

* Corresponding author. Tel.: +1 614 733 3330; fax: +1 614 733 3301.
E-mail address: tonkovich@velocys.com (A.L.Y. Tonkovich).

0920-5861/$ – see front matter
doi:10.1016/j.cattod.2006.07.022

with contact times less than 10 ms and with commercially interesting conversions have been experimentally described in the literature for a number of chemistries, including oxidation, reforming, forward and reverse water gas shift, and ammonia decomposition. Most of the relevant literature describes compact reaction systems that include microchannel or microstructured reactors. Several references cite fast reactions in monolith or gauze type reactors [3]. Microreactors have long been offered as a route to scale-up or commercialize fast reactions as a result of their intrinsic ability to manage the rising challenges of heat and mass transport that accompany reductions in contact time.

Several partial oxidation reactions have been shown experimentally to operate with a contact time less than 10 ms, including the partial oxidation of methane [3–7], ethane [8,9,33], propane [10], butane and higher hydrocarbons [11], several light paraffins [12], and hexane [13].

Several steam reforming reactions at less than 10 ms also have been described in the literature, including integrated methane reforming and methane combustion on adjacent Microchannels [1,14–17,34], methane reforming on highly active catalysts [18], propane reforming [19], butane reforming [20], isooctane reforming [21], and reforming of a host of other high molecular weight hydrocarbons [22].

Other reactions that have been demonstrated at less than 10 ms include the reverse water gas shift reaction [23], ethanol partial oxidation [24], water gas shift [25], hydrogen oxidation [26–29], ammonia decomposition [30], and carbon monoxide oxidation [31]. Combustion of methane with contact times less than 10 ms has been described to support ethane dehydrogenation operating near 50 ms [32]. No references were found with experimental results at less than 1 ms contact time except for high temperature hydrogen oxidation reactions [26].

This study demonstrates that a sufficiently fast catalyst is available to allow methane steam reforming to be carried out with a contact time less than 1 ms. Further reductions in contact time may be reasonably achieved by increasing the catalyst thickness in a manner that minimizes heat and mass transport limitations through careful design. In this work, steam reforming at contact times of 90–900 μm was carried out; the 900 μs contact time tests reached greater than 99% approach to equilibrium conversion and selectivity, while the 90 μm test demonstrated 21% approach to equilibrium.

This study further explores, through the use of simulations, the important variables for pushing the performance of steam reforming in a microchannel reactor. Careful selection of catalyst thickness, porosity, tortuosity, effective thermal conductivity, and open flow gap above the catalyst provides a method to achieve near equilibrium conversion at a contact time of 500 μm.

3. Experimental

3.1. Reactor hardware

Two identical single channel microreactors with adjacent cross-flow combustion channels were built from Inconel 625 metal and operated. The test device (see Fig. 1) included a single 11.4 mm long open reactor channel with a 0.356 open gap that reduced to a 0.076 mm open gap for reactant flow after the 0.28 mm thick catalyst was inserted next to the heat transfer wall. The channel had a width of 10.7 mm. The steam reforming catalyst was held against one heat transfer wall by two Inconel strips of metal along the sides of the catalyst insert that extended across the 0.076 mm gap such that good thermal contact between the catalyst and the microchannel was maintained. The catalyst slurry was ex situ washcoated on a FeCrAlY felt substrate (Technetics), resulting in a total catalyst loading of 0.0125 g, as measured after calcination at 350 °C. The washcoat slurry contained 10 wt% Rh/4.5 wt% MgO/85.5 wt% Al_2O_3, where the synthesis method has been described in detail [15]. Steam reforming process gas flowed in one channel adjacent to the catalyst insert which was pressed next to a heat transfer wall.

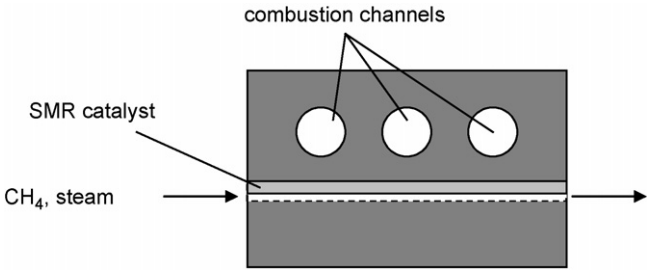

Fig. 1. Schematic of experimentally tested single channel microreactor. Thermocouples are placed in the metal between the reforming channel and the combustion channels.

The heat transfer channels consisted of three parallel cross-flow oriented cylindrical (2.54 mm diameter) channels in which catalytic hydrogen combustion occurred, providing heat to the fast steam reforming reaction. A wall thickness of 1.52 mm separated the SMR process channel and the tangent plane intersecting the edge of the combustion channels. The combustion gas mixture was not pre-mixed, but rather the hydrogen fuel was fed into the air stream through a small jet (circular cross-section, 0.254 mm in diameter) immediately upstream (0.76 mm) of the start of the SMR process channel. To overcome potentially poor mixing of the hydrogen and air in the 2.54 mm cylindrical channels, a static mixer was inserted into each prior to heat treatment. Each static mixer consisted of two offset spiral twisted strips of Inconel 625 with a 2.54 mm diameter such that the created flow pattern was tortuous to enhance mixing. Before SMR catalyst insertion and application of the combustion catalyst to the combustion channel, the device was heat treated in air at 950 °C for 2 h. The combustion catalyst was applied to the heat treated combustion channel interior walls and static mixer surfaces by soaking for two minutes at room temperature in a 10 wt% palladium nitrate solution. The device was then dried at 100 °C for 30 min followed by calcination at 850 °C for 1 h. After the combustion catalyst was applied to the combustion channels, the steam reforming catalyst was inserted into the steam reforming channel and the header and footer connections were welded to the device.

A molar ratio of 3 to 1 steam to methane feed was maintained at total flow rates of 0.61 SLPM to 6.2 SLPM (standard liters per minute at 0 °C and 1 bar) which equate to contact times of about 90–900 μm. Heat transfer wall temperatures were measured by thermocouples in the metal wall between the SMR and combustion channels in three locations along the SMR flow length. Outlet pressure and average heat transfer wall temperature for the 900 μs condition were 12.9 bar and ~840 °C and for the 90 μs condition were 11.4 bar and 810–745 °C (the reactor was much less isothermal at 90 μm corresponding to the heat transfer challenge of further intensification of the microchannel reactor). Inlet gases were preheated to 835 and 765 °C for the 900 and 90 μs conditions, respectively.

The contact time was calculated as follows:

$$\text{contact time} = \frac{\text{open channel volume}}{\text{flow rate at STP}} \quad (1)$$

where channel volume is the volume through which gas flows adjacent to the catalyst and the flow rate at STP is the total inlet flow of reactants calculated at 0 °C and 1 bar.

Inlet gas flows were metered via a Brooks mass flow meter and steam was produced by continuous vaporization of a water stream metered by a high pressure liquid chromatography (HPLC) pump. Dry outlet gas concentrations were measured by gas chromatograph (Agilent), which was calibrated daily. Dry outlet flow rate was measured by dry test meter. The approach to equilibrium methane conversion (which may be expressed as a fraction or a percent) was calculated as

$$\chi_{CH_4} = \left(\frac{y_{CO} + y_{CO_2}}{y_{CO} + y_{CO_2} + y_{CH_4}} \right)_{\text{dry outlet gas}} \quad (2)$$

$$\text{approach} = \frac{(\chi_{CH_4})_{\text{measured or predicted}}}{(\chi_{CH_4})_{\text{equilibrium at } T,P}} \quad (3)$$

where y_i is the mole fraction of species i in the dry outlet gas stream. Equilibrium values for the dry outlet mole fractions were calculated using the NASA-Lewis equilibrium code for the inlet composition (3:1 steam to methane) at the process channel outlet pressure and the average temperature in the heat transfer wall.

3.2. Reactor model development

Optimal regions of performance were found using a designed matrix of computational fluid dynamics (CFD) simulations. Each designed simulation was intended to cover one range of interest for four typical variables of interest, chosen from the following: external flow-by gap adjacent to the catalyst, fluid flow rate, catalyst thickness, catalyst tortuosity, catalyst effective thermal conductivity, and catalyst activity gradient in the flow direction.

Each designed simulation was set up and analyzed using Design Expert® (Stat-Ease®) to predict the effect of varying four independent variables at once, each over a limited range. In this way, the simulation space was adequately covered with a minimal number of CFD runs with a hybrid response surface design (16 runs), plus two additional runs to better estimate the lack of fit. By limiting the range of each variable, a quadratic (second order) fit described the effect of each of the four variables. In all, two designed sets of 18 simulations each were performed, as summarized in Table 1. For each set of simulations, a constant wall temperature boundary condition was assumed. While the assumption of constant wall temperature is challenging to rigorously achieve experimentally, it was viewed as a reasonable starting point in light of previous experimental results [1] where a temperature range of 835–880 °C was maintained over 178 mm reactor length. Each simulation assumed a symmetry plane down the center line of the microchannel that consisted of an open gap for reactant flow adjacent to an engineered porous catalyst—similar to the experiments. The other dimensions of the reaction channel were held constant at 4.06 mm (width) and 177.8 mm (axial length).

Table 1
Ranges of conditions modelled for each set of simulations analyzed, where values in bold represent the simulation range

	Set 1	Set 2
Space velocity (ms^{-1})	**0.24–2.0**	**0.24–2.0**
Flow-by gap (mm)	**0.178–0.762**	**0.356–1.27**
Average catalyst thickness (mm)	**0.0762–0.33**	0.127
Catalyst activity slope (axial direction)	0	**−1 to 1**
Porous catalyst structure effective thermal conductivity (W/(m K))	**0.7–3.0**	1.5
Catalyst pore tortuosity	2	**2–10**
Wall temperature (°C)	840	850

The simulations show the interaction between the various resistances to methane conversion, namely internal mass transport (tortuosity and catalyst thickness), external mass transport (gap size and flow rate), heat transport (thermal conductivity), and reactivity (catalyst thickness and catalyst kinetic factor slope). The value for effective thermal conductivity of the porous catalyst structure was set to vary slightly around 1 W/(m K) to explore performance in the actual range for the porous catalyst structures from Technetics that were used experimentally.

3.3. CFD model runs

A commercial CFD package (Fluent™) was employed to analyze the reforming reactions in microchannel reactors. The general mass, momentum, and energy conservation equations are solved together with user specified reaction kinetics.

4. Chemistry and kinetics

Methane steam reforming (SMR) reaction in a microchannel reactor is the focus of this study. The water gas shift (WGS) reaction also is included as it occurs on the SMR catalyst.

$$CH_4 + H_2O \Leftrightarrow CO + 3H_2 \quad (4)$$

$$CO + H_2O \Leftrightarrow H_2 + CO_2 \quad (5)$$

The following kinetics are used throughout this work:

$$r_1 = k_1\left(P_{CH_4}P_{H_2O} - \frac{P_{CO}P_{H_2}^3}{K_1}\right) \quad (6)$$

$$r_2 = k_2\left(P_{CO}P_{H_2O} - \frac{P_{H_2}P_{CO_2}}{K_2}\right) \quad (7)$$

The reaction rates are in kmol/m^3 cat s, and the pressures P_i in the above equations are in bar. The reaction rate constants are given in the following Arrhenius-form equations:

$$k_1 = A_1 \exp\left(-\frac{E_1}{RT}\right) \quad (8)$$

$$k_2 = A_2 \exp\left(-\frac{E_2}{RT}\right) \quad (9)$$

The activation energy for SMR reaction, E_1 = 1.695E8 J/kmol; and for WGS reaction, E_2 = 6.713E+7 J/kmol. The pre-exponential factors are A_1 = 1.275E+08 and A_2 = 1.466E+03.

K_1 and K_2 are the chemical equilibrium constants given in the following equations:

$$K_1 = \exp\left(\frac{-26830}{T} + 30.114\right) \quad (10)$$

$$K_2 = \exp\left(\frac{4400}{T} - 4.036\right) \quad (11)$$

The parameters in the rate expressions were obtained by fitting kinetic data for a similar rhodium on Mg-spinel catalyst, where the catalyst is described in the literature [15,18].

4.1. Domain geometry

In the endothermic microchannel methane reforming reactor, heat is provided by combustion in adjacent microchannels. For this work, the methane reforming channel was evaluated and a constant temperature thermal boundary condition was imposed on the wall to simulate the adjacent combustion. These simulations did not consider the effect of external heat transfer resistance outside of the reforming channel. This assumption will become more significant as the reaction is further intensified.

Fig. 2 shows a schematic of the methane reforming reactor packed with structured catalyst.

Except for the two cases where the experimental reactor was directly modeled and compared to experimental results, the reaction channel width was held constant at 4.06 mm and the channel length held constant at 177.8 mm for the parametric model study. Other variables were allowed to vary as described in Table 1.

4.2. Boundary conditions

Pressure is set at 23.5 bar at the outlet, unless specified otherwise. Constant temperature is imposed on the channel walls. For all the cases considered, the wall temperature is the same as the feed temperature.

The catalyst structure is modeled as porous media where chemical reactions take place. The complex interaction between mass/heat transfer, as well as chemical reactions within the catalyst structure, lead to internal catalyst temperature and species concentration distributions.

An entrance length equal to 20 times the open channel gap was imposed upstream of the catalyst to avoid an entrance region effect in comparing reactor performance under different variables. For commercial microchannel reactors of interest, a heat exchanger is upstream of the reactor section for preheat and thus the flow field is fully developed and laminar.

4.3. Mesh

A section of a typical mesh is shown in Fig. 3. The higher grid line density within the catalyst structure reflects the understanding that temperature and species concentrations gradients inside the catalyst structure will be greater than those in the flow-by gap. Three meshes of the same structure as shown in Fig. 3 are built with varying level of refinement to verify the mesh independency of the CFD solution.

4.4. Material properties

The mixture of interest was composed of methane (CH_4), steam (H_2O), hydrogen (H_2), carbon monoxide (CO), and carbon dioxide (CO_2). Ideal gas was assumed in calculating the density of the mixture. The heat capacity, thermal conductivity, and viscosity of the mixture were calculated as a mass-weighted average of the values for each constituent. The material properties of each individual species were assumed to be, in general, functions of the local temperature. The exception to this was the mass diffusivity of each individual species. For part

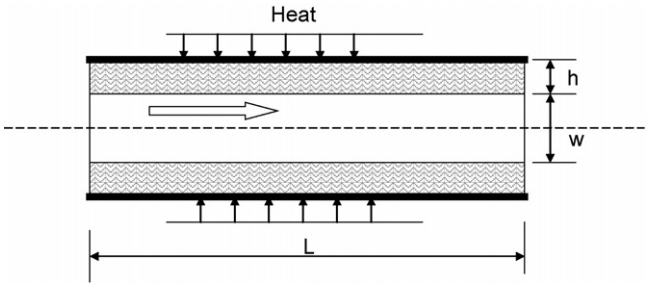

Fig. 2. Microchannel reactor domain for CFD runs.

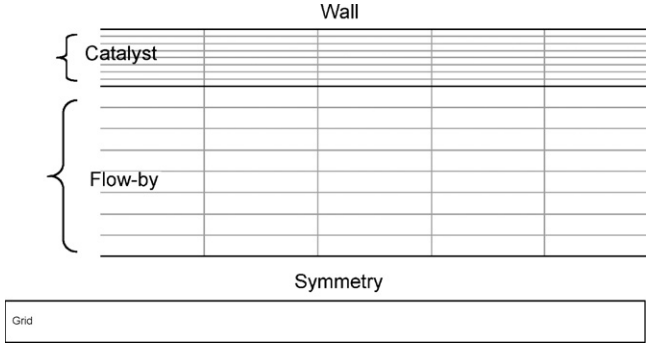

Fig. 3. Mesh used in CFD simulations.

Table 2
Mass diffusivity, D (m^2/s), of reactant and product species

CH_4	1.03E−5
H_2O	1.7E−5
H_2	3.44E−5
CO	1.01E−5
CO_2	7.67E−6

of the modeling cases, when the reactor wall temperature and the feed inlet temperature were specified at 850 °C, the mass diffusivity of each species was assumed to be independent of the temperature. The error introduced by this simplification is small since the temperature variation within the reactor is less than 20 °C. The actual values used are the values of the mass diffusivity which were calculated at 850 °C using Chemcad™—a process simulation package, and are shown in Table 2.

When solving the species mass transport equations, binary mass diffusion coefficients were used directly. In other words, a dilute system was assumed and considered reasonable as excess steam was present.

4.5. Characteristics of the catalyst structure

For flow simulation in the catalyst structure, Darcy's law was used. The following parameters were provided to the CFD code:

α: permeability
C: inertial resistance factor

These parameters may be defined differently based upon different coordinate directions. In this work, only isotropic catalyst structures were considered and the factors α and C are held constant.

$$\nabla p = -\frac{\mu}{\alpha} v - C\left(\frac{1}{2}\rho v^2\right) \tag{12}$$

The effective thermal conductivity of the catalyst structure system including the porous structure and intervening gas was calculated using the following equation:

$$k_{\text{eff}} = \gamma k_{\text{f}} + (1-\gamma) k_{\text{s}} \tag{13}$$

γ is the porosity of the porous medium, k_{f} the fluid phase thermal conductivity, and k_{s} is the porous medium effective thermal conductivity as measured in air at ambient conditions.

γ was assumed to be 0.5 and k_{s} was varied as shown in Table 1, while Fluent calculated the k_{f} of the mixture based on the thermal conductivity of all species and the mixing law. The value of the porous medium effective thermal conductivity was measured to be around 1 W/(m K) in air at ambient conditions.

In general, both the bulk and Knudsen diffusion were assumed to contribute to the mass transport rate within the pore volume. For equimolal binary counter-diffusion, the effective diffusivity was calculated as

$$D_{\text{eff}} = \frac{1}{1/D_{\text{e}} + 1/D_{\text{k}}} \tag{14}$$

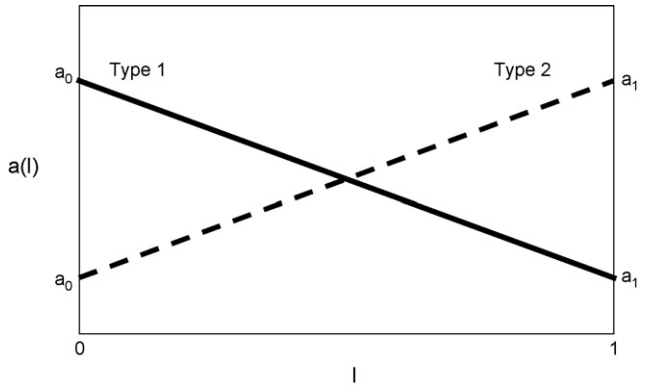

Fig. 4. Catalyst activity distributions in axial direction. L is the axial location normalized by the reactor total length ($l = 0$ at the upstream end of the reactor, $l = 1$ at the downstream end of the reactor).

where D_{eff} is the effective diffusivity within the porous medium, D_{e} the bulk diffusivity in the pore, and D_{k} is the Knudsen diffusivity.

The bulk diffusivity of each species i in the pores of the porous medium is affected by the connection of the pores of different sizes. A simple parallel pore model yields the following equation for the effective bulk diffusivity:

$$D_{\text{e}} = \frac{D_i}{\delta} \tag{15}$$

D_i is the molecular mass diffusivity of species i and δ is the tortuosity factor of the porous medium.

The catalyst support structure of interest in this study possesses larger than average pore size compared to a catalyst pellet. The mean opening of the porous support structure was of the order of 20 μm. The contribution from the Knudsen diffusion is calculated to be relatively small. The tortuosity factor was not known for the felt-like porous catalyst support structure, and as such this parameter was allowed to vary in the simulation matrix.

4.6. The non-uniform catalyst activity distribution

For the structured catalyst, the catalyst activity distribution was varied in the axial direction, where more catalyst is at either the end or front of the catalyst length in either a linearly increasing or decreasing function respectively (shown in Fig. 4).

The distribution function $a(r)$ is shown in the figure.

Table 3
CFD predictions for experimental run points

	Case 1	Case 2
CH_4 flow rate (SLPM)	0.153	1.55
Steam flow rate (SLPM)	0.461	4.74
Total flow (SLPM)	0.614	6.29
Outlet pressure (bar)	12.63	11.14
Temperature (°C)	835	806
Predicted conversion (%)	71.5	13.3
Contact time (μs)	900	90
Equilibrium conversion at temperature (%)	89.1	86.4
Predicted approach to equilibrium (%)	80	15

Table 4
Experimental microchannel reactor results

	1	2
SMR contact time (μs)	900	90
Time on stream for sample (h)	73	10
Molar steam to carbon ratio	3.0	3.0
Percent excess combustion air (%)	450	260
Inlet flows and compositions		
SMR CH_4 flow rate (SLPM)	0.153	1.55
SMR steam flow rate (SLPM)	0.461	4.64
Air flow rate (SLPM)	5.4	5.0
Fuel H_2 flow rate (SLPM)	0.508	0.81
Gas stream temperatures		
SMR inlet gas temperature (°C)	837	788
SMR outlet gas temperature (°C)	802	754
Air inlet gas temperature (°C)	806	732
Exhaust gas temperature (°C)	912	862
Gas stream pressures and pressure drops		
SMR inlet pressure (bar)	13.0	13.0
SMR outlet pressure (bar)	12.9	12.1
SMR pressure drop (bar)	0.1	0.9
Air inlet pressure (bar)	1.47	1.43
Air pressure drop (bar)	0.13	0.1
SMR performance		
SMR CH_4 conversion (GC, %)	88.2	17
Selectivity: CO (%)	38.3	43
Average reactor web temperature (°C)	837	811
Equilibrium conversion at temperature (°C)	89.1	86.4
Approach to equilibrium (%)	99	19.7
Average heat flux (W/cm^2)	18.9	21.3
Combustion performance		
Combustion H_2 conversion (%)	100	100

5. Results and discussion

5.1. Experimental

The results of the single channel microreactor CFD simulations are shown in Table 3, while the experimental results are presented in Table 4.

At 837 °C average reactor temperature and 12.9 bar (outlet pressure) with 3:1 steam to carbon ratio at 900 μs contact time (0.62 SLPM) a methane conversion of 88% was observed, an approach of more than 98% to equilibrium. The corresponding CFD run predicted 80% approach to equilibrium.

At 811 °C average reactor temperature and 12.1 bar (outlet pressure) with 3:1 steam to carbon ratio at 90 μs contact time (6.2 SLPM) a methane conversion of 17% was observed, which is an approach of 19.7% to equilibrium. The corresponding CFD run predicted 15% approach to equilibrium. Fig. 5 shows the time on stream plot for this case, where the catalyst performance was fairly stable over 200 h.

CFD simulations of experimental conditions assumed an effective thermal conductivity of 1.8 W/(m K) and a tortuosity factor of 2. Also assumed is that the catalyst is equally disposed within the wall structure laterally. An entrance length of 20 equivalent diameters was included in the simulation while the experiments introduced the reactant directly into the microchannel.

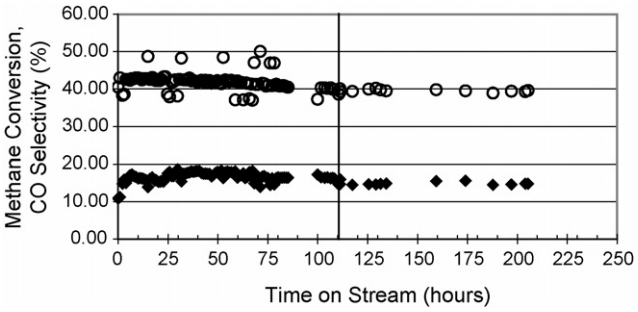

Fig. 5. Time on stream performance for 90 μs case where conversion is shown with the filled diamonds and selectivity to CO with open circles. At 110 h TOS an upset (shown with a vertical bar) occurred, where the hydrogen fuel was lost to the combustion side of the reactor.

The experimental results exceed the model simulations and suggest that the selected reaction kinetics may be somewhat conservative. The CFD simulations are considered valid for predicting trends and highlighting the importance or lack of importance of several key variables.

5.2. Model predictions

The model predictions are presented as iso-approach to equilibrium curves for a host of variables. The predictions are taken from the statistical analysis of the CFD simulations.

A typical parity plot comparing curve-fit-based predictions of the statistical data (model) analysis to actual CFD simulation results is shown in Fig. 6. The second order curve fits were obtained by backward elimination assuming an alpha-out value of 0.05 to eliminate statistically insignificant parameters. The parity plot shows excellent agreement between the actual CFD runs and the fit values from statistical analysis. As such,

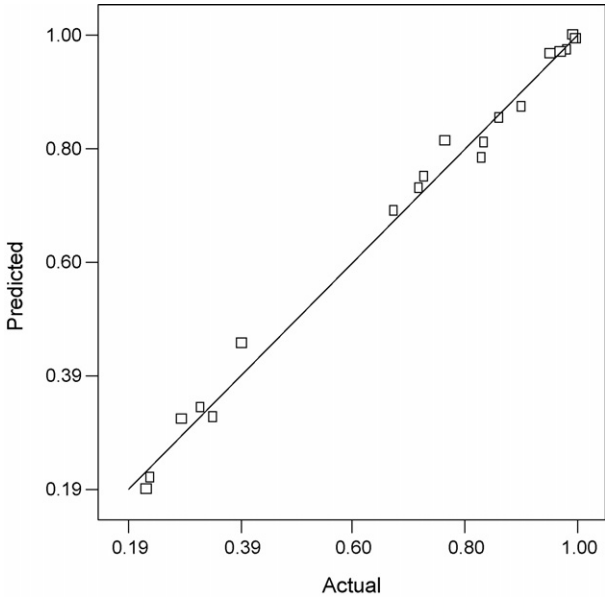

Fig. 6. Parity plot of SMR reaction approach to equilibrium methane conversion predicted via quadratic curve fit of CFD predictions versus actual CFD predictions for the conditions of Set 1 in Table 1.

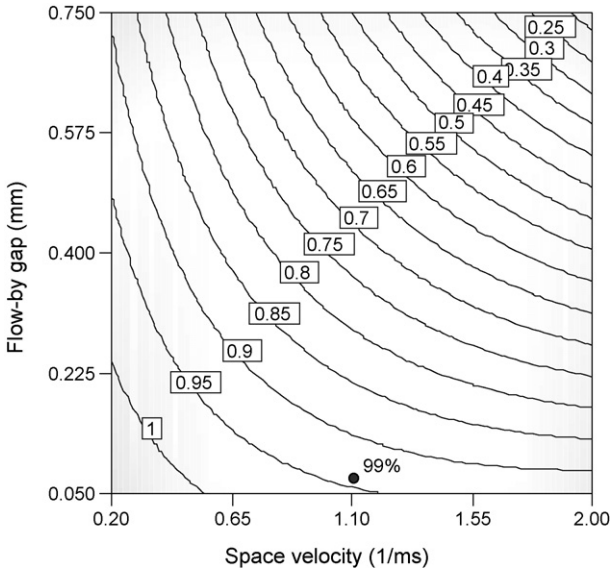

Fig. 7. Predicted SMR reaction approach to equilibrium methane conversion for the conditions of Set 1 in Table 1, with a constant thermal conductivity of 0.9 W/(m K), and a catalyst thickness of 0.28 mm.

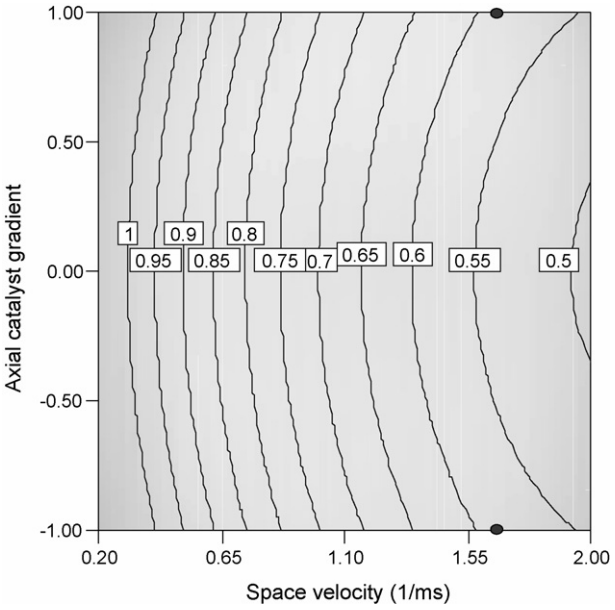

Fig. 9. Predicted SMR reaction approach to equilibrium *methane conversion* for the conditions of Set 2 in Table 1, with a 0.36 mm flow-by gap, and a constant catalyst pore tortuosity of 2.

confidence in the statistical analysis allowed for investigating the effect of several parameters.

5.3. Flow-by gap

The impact of the gap above the catalyst for reactant flow is a significant factor in the performance of the microchannel reactor. Small gaps reduce diffusional resistance, while large gaps exacerbate diffusional resistance. For laminar flow microchannel reactors, the flow-by gap will always be an important variable in reactor performance when the microchannel is run with short contact times.

Fig. 7 shows the effect of space velocity (or flow rate) and flow-by gap (or diffusional distance) on the predicted approach to equilibrium methane conversion for a fixed catalyst thickness (0.28 mm) and catalyst thermal conductivity (∼0.9 W/(m K)). The experimental results collected at 900 μm are shown by the dot in Fig. 7.

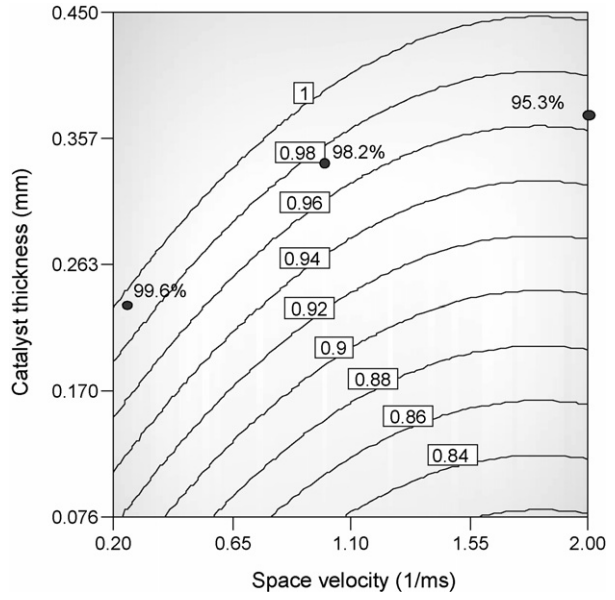

Fig. 8. Predicted SMR reaction approach to equilibrium methane conversion for the conditions of Set 1 in Table 1, with a constant thermal conductivity of 1.85 W/(m K), and a flow-by gap of 0.05 mm (labels on dots indicate actual CFD simulation predicted percent approach to equilibrium, contours show curve-fit-predicted fractional approach to equilibrium).

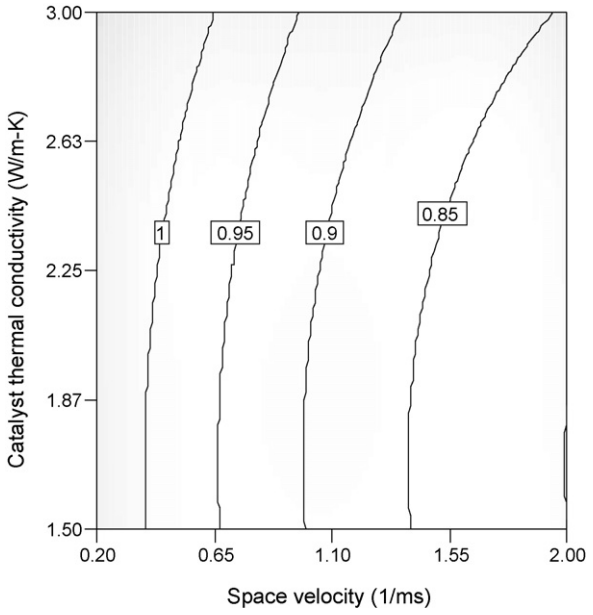

Fig. 10. Predicted SMR reaction approach to equilibrium methane conversion for the conditions of Set 1 in Table 1, with a constant catalyst thickness of 0.37 mm, and a flow-by gap of 0.2 mm.

Table 5
Summary of microchannel reactor design variables

Variable	Importance	Range of study	Notes and caveats
Flow-by gap	High	0.05–0.75 mm	Increasing importance with decreasing contact time for laminar flow
Catalyst thickness	High	0.075–0.45 mm	Increasing thickness yields enhanced performance; provided minimal internal heat and mass transport resistance
Axial gradient in catalyst activity	Low	Linearly increasing or linearly decreasing	Little impact for isothermal wall; large impact expected for non-isothermal wall
Effective thermal conductivity	Low	1.5–3 W/(m K)	Little impact as long as sufficiently high; large impact expected at reduced values

The simulations show the importance of both the flow-by gap and space velocity on the approach to equilibrium. As the space velocity increases at equal gap, the approach to equilibrium drops as one would expect from an increased demand on the available number of catalyst sites. As the flow-by gap increases at equal space velocity, the drop in approach to equilibrium is more pronounced resulting from an increase in the external mass transfer resistance and an increased demand on the fixed number of catalyst sites. The diffusional distance of reactants to the catalyst wall increases with the flow-by gap and the effective or apparent activity of the catalyst is reduced.

Thus the challenge for realizing high apparent catalyst activity becomes much greater as the microchannel gap is increased. As the space velocity increases, the contribution from external mass transfer resistance becomes more important as denoted by a closer spacing of the iso-approach lines on the right hand side of Fig. 7.

5.4. Catalyst thickness

The impact of catalyst thickness was surprising, as shown in Fig. 8. The overall approach to equilibrium could be increased at surprisingly thicker catalysts, as long as the catalyst effective thermal conductivity was held high (*minimize internal heat transfer resistance*) and the tortuosity was relatively low (*minimize internal mass transfer resistance*). In this simulation, the tortuosity was held at 2.

For these simulations, the activity per unit thickness was held constant. Thus thicker catalysts added additional active sites to convert the reactants. The additional sites were generally accessible and contributed to the reaction provided that internal heat and mass transfer limitations did not dominate. The important consideration is *how* the active sites are added. For tortuosity values greater than 5, any increase in the catalyst thickness over 0.2 mm had little impact in increasing the approach to equilibrium.

The predicted performance suggests that a space velocity of 2 (ms^{-1}) or 500 μm near equilibrium performance could be achieved with a catalyst thickness approaching 0.45 mm. This performance prediction is predicated on a very low tortuosity catalyst support (2) and a fairly high effective thermal conductivity of the support (1.85 W/(m K)).

5.5. Axial gradients in catalyst loading

The axial gradient in the catalyst thickness as modeled in Fig. 4 is shown in Fig. 9. The axial gradient in catalyst activity was found to have little effect on the predicted approach to equilibrium in the range covered by the simulations—as long as the total amount of catalyst is held constant.

Axial gradients in the location of the catalyst had little impact on the overall approach to equilibrium. While these results are somewhat surprising in that applying more catalyst near the front of the kinetically-limited reaction had little impact on overall conversion, they do suggest that the isothermal wall assumption may mask underlying behavior. This catalyst is allowed to consume as much heat as required from the wall boundary condition, while a real system may be limited by the local heat flux along the reactor length in addition to the actual non-isothermal wall profile. As such, a modified boundary condition might reveal more interesting behavior for this axial catalyst gradient variable. It is further noted that the practical implementation of a tailored axial catalyst loading may be challenging to achieve.

5.6. Effective thermal conductivity

The effective thermal conductivity of the engineered porous catalyst plays a less important role as long as it is sufficiently high. Fig. 10 shows the behavior over the range of 1.5–3 W/(m K).

Effective thermal conductivity for a porous catalyst engineered support structure played little role in the overall approach to equilibrium. This suggests that for the range of contact times evaluated, there was little heat transfer resistance. One would expect this variable to become more important as the contact time is further reduced and the heat load increases. This variable also will become important if the actual effective thermal conductivity of the catalyst structure is below the values investigated with this study.

5.7. Summary of microchannel design variables

Four variables were evaluated for their impact on the design and performance of microchannel reactors toward the aim of further process intensification. Table 5 summarizes the four primary variables with notes and caveats for reactor contact times from 5 ms to 500 μm.

6. Conclusions

Methane steam reforming experiments were conducted at contact times below 1 ms to demonstrate that the tailored design

of microchannel reactors enable high rates of heat transfer and mass transfer to support fast reactions. Specifically, experiments at 90 and 900 μm were conducted in a 0.28 mm thick porous catalyst structure held adjacent to a 0.076 mm flow gap, where greater than 98% approach to equilibrium was demonstrated at 900 μm and with good model agreement. At 90 μm, 19.7% approach to equilibrium is measured and 15% approach to equilibrium is predicted. Additional model sensitivity results suggest that a high approach to equilibrium could also have been achieved with the same rhodium on MgO catalyst at 500 μm, if the catalyst were washcoated on a thick porous catalyst structure of up to 0.45 mm. Further, the model suggests that the flow-by gap and catalyst thickness are two important variables to optimize microchannel reactor performance.

Acknowledgements

The authors gratefully acknowledge the financial support of Velocys and commercial partners in funding development of novel high intensity catalytic reactors and for permission to publish this work.

References

[1] A.Y. Tonkovich, S. Perry, Y. Wang, D. Qiu, T. LaPlante, W.A. Rogers, Microchanel process technology for compact methane steam reforming, Chem. Eng. Sci. 59 (22–23) (2004) 4819–4824.
[2] S. Bharadwaj, L.D. Schmidt, Catalytic partial oxidation of natural gas to syngas, Fuel Process. Technol. 42 (1995) 109–127.
[3] D. Hickman, L.D. Schmidt, Production of syngas by direct catalytic oxidation of methane, Science 259 (5093) (1993) 343–346.
[4] D. Hickman, E. Haupfear, L.D. Schmidt, Synthesis gas formation by direct oxidation of methane over Rh monoliths, Catal. Lett. 17 (1993) 223–237.
[5] C. Goralski, R. O'Connor, L.D. Schmidt, Modeling homogeneous and heterogeneous chemistry in the production of syngas from methane, Chem. Eng. Sci. 55 (2000) 1357–1370.
[6] S. Reyes, J. Sinfelt, J. Feeley, Evolution of processes for synthesis gas production: recent developments in an old technology, Ind. Eng. Chem. Res. 42 (2003) 1588–1597.
[7] D. Neumann, G. Veser, Catalytic partial oxidation of methane in a high-temperature reverse flow reactor, AIChE J. 51 (1) (2005) 210–223.
[8] M. Huff, L.D. Schmidt, Ethylene formation by oxidative dehydrogenation of ethane over monoliths at very short contact times, J. Phys. Chem. 97 (45) (1993) 11815–11822.
[9] D.W. Flick, M.C. Huff, Oxidative dehydrogenation of ethane over a Pt-coated monolith versus Pt-loaded pellets: surface area and thermal effects, J. Catal. 178 (1998) 315–327.
[10] I. Aartun, T. Gjervan, H. Venvik, O. Gorke, P. Pfeifer, M. Fathi, A. Holmen, K. Schubert, Catalytic conversion of propane to hydrogen in microstructured reactors, Chem. Eng. J. 101 (2004) 93–99.
[11] L.D. Schmidt, E.J. Klein, C.A. Leclerc, J.J. Krummenacher, K.N. West, Syngas in millisecond reactors: higher alkanes and fast lightoff, Chem. Eng. Sci. 58 (3–6) (2003) 1037–1041.
[12] A. Beretta, P. Forzatti, Partial oxidation of light paraffins to synthesis gas in short contact-time reactors, Chem. Eng. J. 99 (2004) 219–226.
[13] R. O'Connor, E. Klein, L.D. Schmidt, High yields of synthesis gas by millisecond partial oxidation of higher hydrocarbons, Catal. Lett. 70 (3–4) (2000) 99–107.
[14] T. Mazanec, Microchannel technology for gas to liquids conversion, Petrochem. Gas Process. Q. (2003) 149–153.
[15] A. Tonkovich, G. Roberts, F. Sean, P. Neagle, D. Qiu, M. Schmidt, S. Perry, D. Hesse, R. Luzenski, B. Chadwell, Y. Peng, N. Gano, R. Long, W. Rogers, R. Arora, W. Simmons, B. Yang, D. Kuhlmann, Y. Wang, T. Yuschak, T. Forte, J. Monahan, R. Jetter, Integrated combustion reactors and methods of conducting simultaneous endothermic and exothermic reactions, US patent application US2004/0033455A1 (2004).
[16] A.Y. Tonkovich, D. Kuhlman, A. Rogers, J. McDaniel, S. Fitzgerald, R. Arora, T. Yuschak, Microchannel technology scale-up to commercial capacity, Chem. Eng. Res. Des. 83 (A6) (2005) 634–639.
[17] K. Jarosch, A.Y. Tonkovich, S. Perry, D. Kuhlman, Y. Wang, Microchannel reactors for intensifying gas-to-liquid technology, in: Y. Wang, J.D. Holladay (Eds.), Microreactor Technology and Process Intensification (ACS Symposium Series), 2005.
[18] Y. Wang, Y. Chin, R.T. Rozmiarek, B.R. Johnson, Y. Gao, J.M. Watson, A.Y. Tonkovich, D.P. Vanderwiel, Highly active and stable Rh/MgO-Al_2O_3 catalysts for methane steam reforming, Catal. Today 98 (4) (2004) 575–581.
[19] G. Kolb, R. Zapf, V. Hessel, H. Lowe, Propane steam reforming in microchannels—results from catalyst screening and optimization, Appl. Catal. A Gen. 227 (2004) 155–166.
[20] E. Daymo, D. VanderWiel, S. Fitzgerald, Y. Wang, R. Rozmiarek, M. LaMont, A.Y. Tonkovich, Microchannel fuel processing for man portable power, in: Proceedings of the Fourth International Conference on Microreaction Engineering, Atlanta, GA, (2000), pp. 364–369.
[21] S. Fitzgerald, R. Wegeng, A.Y. Tonkovich, Y. Wang, H. Freeman, J. Marco, G. Roberts, D. VanderWiel, A compact steam reforming reactor for use in an automotive fuel processor, in: Proceedings of the Fourth International Conference on Microreaction Engineering, Atlanta, GA, (2000), pp. 358–363.
[22] A.Y. Tonkovich, Y. Wang, Overview of early-stage microchannel reactor development at Pacific Northwest National Laboratory, in: Y. Wang, J.D. Holladay (Eds.), Microreactor Technology and Process Intensification (ACS Symposium Series), 2005.
[23] D. VanderWiel, J. Zilka-Marco, Y. Wang, A.Y. Tonkovich, R. Wegeng, Carbon dioxide conversions in microreactors, in: Proceedings of the Fourth International Conference on Microreaction Engineering, Atlanta, GA, (2000), pp. 187–193.
[24] G. Deluga, J. Salge, L.D. Schmidt, X. Verykios, Renewable hydrogen from ethanol by autothermal reforming, Science 303 (2004) 993–997.
[25] A.Y. Tonkovich, J.L. Zilka, M.J. LaMont, Y. Wang, R.S. Wegeng, Microchannel reactors for fuel processing applications. I. Water gas shift reactor, Chem. Eng. Sci. 54 (13–14) (1999) 364–371.
[26] M. Hersch, Hydrogen–oxygen chemical reaction kinetics in rocket engine combustion, NASA Technical Note, NASA TN D-4250 (1967).
[27] G. Veser, G. Friedrich, M. Freygang, R. Zengerle, A micro reaction tool for heterogeneous catalytic gas phase reactions, in: Twelfth IEEE International Conference on Micro Electro Mechanical Systems, MEMS'99, 1999, 394–399.
[28] G. Veser, Experimental and theoretical investigation of H_2-oxidation in a high-temperature catalytic microreactor, Chem. Eng. Sci. 56 (2001) 1265–1273.
[29] M. Janicke, H. Kestenbaum, U. Hagendorf, F. Schuth, M. Fichtner, K. Schubert, The controlled oxidation of hydrogen from an explosive mixture of gases using a microstructured reactor/heat exchanger and Pt/Al_2O_3 catalyst, J. Catal. 191 (2000) 282–293.
[30] L. Allen, P. Irving, W. Thomson, Microreactor systems for hydrogen generation and oxidative coupling of methane, in: Proceedings of the Fourth International Conference on Microreaction Engineering, Atlanta, GA, (2000), pp. 351–357.
[31] S.K. Ajmera, C. Delattre, M.A. Schmidt, K.F. Jensen, Microfabricated differential reactor for heterogeneous gas phase catalyst testing, J. Catal. 209 (2002) 401–412.
[32] K. Venkataraman, J. Redenius, L.D. Schmidt, Millisecond catalytic wall reactors: dehydrogenation of ethane, Chem. Eng. Sci. 57 (2002) 2335–2343.
[33] A.S. Bodke, D. Henning, L.D. Schmidt, S.S. Bharadwaj, J.J. Maj, J. Siddall, Oxidative dehydrogenation of ethane at millisecond contact times: effect of H_2 addition, J. Catal. 119 (1) (2000) 62–74.
[34] A. Tonkovich, G. Roberts, S. Perry, S. Fitzgerald, Integrated reactors, methods of making same, and methods of conducting simultaneous exothermic and endothermic reactions, US patent application, US2003/0072699A1 (2003).